Computers and Electronics in Agriculture 162 (2019) 380–388

Contents lists available at ScienceDirect

Computers and Electronics in Agriculture

journal homepage: www.elsevier.com/locate/compag

Original papers

Development of an image-based system to assess agricultural fertilizer spreader pattern

André R.S. Marcal[a], Mario Cunha[b,c,*]

[a] Faculdade de Ciências da Universidade do Porto, Departamento de Matemática, Rua do Campo Alegre, 687, 4169-007 Porto, Portugal
[b] Faculdade de Ciências da Universidade do Porto, Departamento de Geociências Ambiente e Ordenamento do Território, rua do Campo Alegre, sn, 4169-007 Porto, Portugal
[c] Institute for Systems and Computer Engineering, Technology and Science INESC TEC, Campus da Faculdade de Engenharia da Universidade do Porto, Rua Dr. Roberto Frias, 4200-465 Porto, Portugal

ARTICLE INFO

Keywords:
Farm machinery
Fertilizers spreaders
Calibration pattern
Image processing

ABSTRACT

An Automatic Calibration of Fertilizers (ACFert) system was developed, for use with centrifugal, pendulum or other types of broadcast spreaders which distribute dry granular agricultural materials on the top of the soil. The ACfert is based on image processing techniques and includes a specially designed mat, which should be placed in the ground for spreaders calibration. A set of images acquired outdoor by a standard device (simple camera) is used to extract information about the spreader distribution pattern. Each image is processed independently, providing as output two numerical values for each grid element present in the image – the number of fertilizers/seeds counted, and its numerical label. The performance of ACFert was evaluated for automatic granules detection using a set of manual counting measurements of nitrate fertilizer and wheat seeds. A total of 185 images acquired with two mobiles devices were used with a total of 498 quadrilateral elements observed and analysed. The overall mean absolute relative error between counting and computed by the ACFert system, were 0.75 ± 0.75% for fertilizer and 2.12 ± 1.68% for wheat. This near real-time calibration tool is a very low cost system that can be easily used on field, providing results to support accurate spreader calibration in near real time for different types of fertilizers or seeds.

1. Introduction

There are agronomic, environmental and economic reasons why the fertilizers should be placed accurately at the right quantity in the field. Nowadays, avoidance of misapplication of fertilizers/seeds is a major multidimensional concern to farmers, machinery developers, as well as the agriculture industry.

Broadcaster centrifugal spreaders are the worldwide most popular farm machine used for dry granular applications such as fertilizer and seeds (Van Liedekerke et al., 2006). The pendulum spreader and pneumatic spreaders are other types of spreaders, that compared with the centrifugal spreader, are much less used, because of the small working width and high costs, respectively (Van Liedekerke, 2007).

Centrifugal spreaders typically have, positioned under a hopper with metering port(s), 2 spinning discs or rotary impeller with deflectors, turning in opposite directions that flings the granules out in an arc, until spread it on the ground in different patterns, after a ballistic flight. The use of two rotary discs helps to provide a pattern distribution on the ground that is symmetrical from both sides, but they do not guarantee a uniform pattern.

The popularity of these agricultural granules applicators lies in their low price, easy maintenance, simplicity, robustness, high field work capacity related to the large working width (more than 36 m) and high work speed, being cheap considering all these advantages. However, the lateral distribution pattern is highly sensitive to machine characteristics (e.g. impellers size, speed), granules properties (e.g. class size, shape, density) and weather conditions (e.g. wind, humidity), all effects that are well documented in Abbou-ou-cherif et al. (2017), Cool et al. (2014), Cool et al. (2016a), Hofstee and Huisman (1990), Olieslagers et al. (1996), Parish (2003). Therefore, these applicators are error-prone, potentially leading to misapplication of fertiliser/seeds, which is often caused by poor calibration.

The calibration of the centrifugal, pendulum or other types of agricultural spreaders to apply dry granular material on the top of the soil, includes the determination of delivery rate (kg/ha) and characterization of the pattern distribution perpendicular to the direction of

* Corresponding author.
E-mail addresses: andre.marcal@fc.up.pt (A.R.S. Marcal), mccunha@fc.up.pt, mario.cunha@inesctec.pt (M. Cunha).

https://doi.org/10.1016/j.compag.2019.04.031
Received 19 June 2018; Received in revised form 7 April 2019; Accepted 23 April 2019

spreader travel. The spreader setting, for a desired delivery rate, should be based on the effective swath width, determined from the pattern distribution data (ASABE, 2004). Triangular and trapezoidal transversal distribution patterns were considered the most appropriated to provide a uniform application when properly overlapped (Griffis et al., 1983; Grift, 2000).

The granular mass application rate is generally controlled by the metering port(s) positioned under the hopper using well established processes. The most employed methods for calibrating the spreader quantity are based on static tests allowing the material to drop into a container. Real time measurements of the quantity of fertilizer that are being spreader can be assessed with image sensors (Back et al., 2014), capacitance sensors (Zhou et al., 2017) or dynamic weighting systems (e.g. Parish, 2006).

The spreader calibration of lateral pattern distribution on the ground is still the critical point to obtain the swath width for optimum uniform distribution adjustment. Despite the high economic, environmental and agronomic worldwide importance of the spreader pattern distribution and the relevant research done on this subject dating back to the 1960's (Inns and Reece, 1962; Mennel and Reece, 1963; Patterson and Reece, 1962), there is no accurate, operational and cheap systems for spreader calibration (Shi et al., 2018).

The most common test for lateral pattern calibration at farm level is done by using a setup of collection trays placed across to the driving direction of the spreader (e.g. Cool et al., 2016b). The collected granules, which contains a sample representing the amount of material per tray area (g m^{-2}), are weighting and the distribution pattern obtained. These tests can also be carried out in specific and sophisticated spreading-halls, where the external factors (e.g. wind, humidity) are limited as much as possible, in order to make experiments more reproducible and comparable (Reumers et al., 2003; Van Liedekerke, 2007). These halls are large and require huge amounts of fertilizers that lose the commercial value after the tests, due to mechanical breakage (Van Liedekerke et al., 2009). Nevertheless, the hall-tests are often used by spreader manufactures to assist farm machinery development and to produce the spreading tables for specific machine that links granules properties, machine regulations and desired pattern distribution, according to international standard systems.

The most common standard testing systems used to obtain spread pattern from spinning disc spreaders are: (i) ISO standard with two versions ISO 5690/1 and 5690/2, (ii) ASAE Standard S341.2 in United States of America, (iii) European Committee for Standardisation CEN. EN 12761-1,2,3, that operated in European Union Countries, (iv) ACCU spread in Australia and (v) Spreadmark in New Zealand. Most of these test methods use 0.5 × 0.5 m trays organised in a single transverse row to capture the spread pattern of the spreader. The effect of tray frequency, tray spacing, and tray size among other test specifications used in different spreader certification norms on the accuracy of results were presented by (Jones et al., 2008; Lawrence et al., 2007).

The uniformity of lateral distribution are commonly evaluated by the coefficient of variation (CV), calculated by listing the data from the individual tray for the centre swath (ASABE, 2004). The simulated field distribution for each swatch width to be evaluated is constructed by accumulating the sample mass from the simulated overlapping swaths at each collection tray location (Grift, 2000). The lower the CV, the more uniform the distribution pattern. If the application rate were exactly the same all the way across the overlapped pattern, the CV should be 0%. Quality assurance programs and standard international test methods accept a transversal uniformity coefficient of variation (CV) of 15% for fertilizer containing nitrogen and 25% for products that do not contain nitrogen.

Because spreader calibration based on the collected measurements are cumbersome, laborious, time-consuming and expensive for the farmer, hence not common practice, several alternatives approaches have been developed to characterize the spreading pattern, which can be classified as: "predicting" trajectory of particles and "mapping" the landed positions of particles. The first approach is generally based on the ballistic flight model or on the cylindrical spread pattern to predict the trajectory of particles leaving the spreading vanes and mapping the putative landing position of individual particles.

The ballistic particle flight models include a number of parameters from spreader settings, particles properties and environment used for calculating the distribution pattern (Aphale et al., 2003; Hofstee and Huisman, 1990; Olieslagers et al., 1996). The cylinder measurements reported by Reumers et al. (2003) is a compact device where the spinning disc is surrounded by a series of cylindrical collector tray in order to capture the spread particles. Subsequently, photogrammetry techniques are used to estimate particles positions and velocities vectors when leaving the disc. By using ballistic flight models, the standard distribution pattern of a certain combination of fertilizer type and spreader (with certain settings) can be estimated. Several authors proposed an approach for spreader pattern characterization, based on a combination of a ballistic flight model and 2D image systems to measure the initial condition of particles flight (velocity and direction) and their size (Grift and Hofstee, 1997). While this 2D image systems could track the characteristics of the particles moving parallel to the image sensor, 3D sensors are needed to catch the different directions of the particles leaving the vane. Hence a 3D approach using a high speed binocular stereovision-based technique has been proposed to improve the determination of particles' characteristics leaving the spreader (Hijazi et al., 2014; Hijazi et al., 2011) including tractor motion, particle size and wind (Cool et al., 2017). While these complex and expensive methods based on predicting granules trajectories can be useful for the knowledge of the physical process involved in the pattern distribution of agricultural granules, and support farm machinery design developments, they are still not operational for accurate calibration of spreaders in the field.

In recent years, advances in digital cameras and image processing techniques have contributed considerably for the calibration of spreader fertilizer patterns based on mapping the landed positions of particles. Hensel (2003) proposed an automatic image system that operates with images acquired directly from the soil surface. In this system, the fertilizer particles are optically distinguished from soil components by their specific differences in colour, shape and size. It was found that the rate of detection is deeply influenced by the fertilizers' nature and environmental factors such as light, condition of soil and disturbing vegetation. Lawrence et al. (2007), proposed a different image-processing method for spreaders that works with images acquired directly from ISO size (0.5 m × 0.5 m) collectors tray. While this approach can be used for accurately calculating the uniformity pattern for the urea fertilizer tested, the performance for other agricultural granules are unknown and they had problems in situations of high application rates.

The literature suggests that image processing techniques have great potential for near real-time calibration of distribution pattern in the field and can be an alternative process for the complex and expensive modelling trajectory based approaches, potentially providing similar information as obtained from tray measurements. Previous works using this approach indicate a number of challenges that need to be addressed in order to have a reliable image processed based spreader calibration system. These include changing illumination conditions, image background used, distance to the target in the image acquisition stage, flexibility to work with different types of agricultural materials (fertilizer and seeds), range of particles size tested, detection of geminated particles that often occur at high application rates, and the combination of multiple images for generating uniformity indices.

This paper presents the ACFert, an automatic image processing tool to measure the spread patterns for use with centrifugal, pendulum or other types of broadcast agricultural spreader to apply dry granular material on the top of the soil. The system envisaged includes a specially designed mat, which should be placed in the ground before fertilizing. A set of images acquired outdoor by a standard device (simple

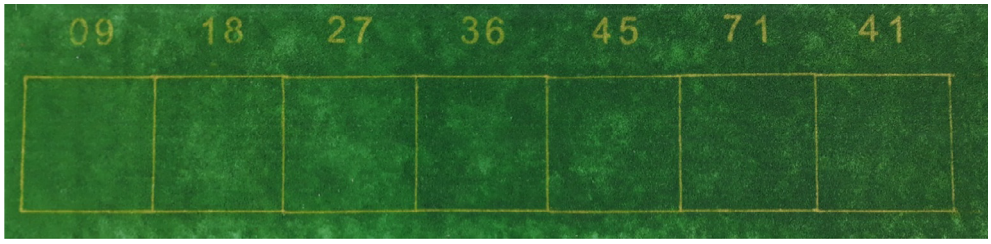

Fig. 1. Prototype calibration mat, with 7 square elements of 0.5 × 0.5 m.

camera) is used to extract information about the spreader distribution pattern. This calibration tool is a very low cost system that can be used on site, providing results to support accurate agricultural fertilizer spreader pattern in near real time for different types of fertilizers or seed.

2. Materials and methods

The procedure developed is based on a calibration mat with a grid of aligned square elements of fixed size. Ideally the material surface should be rough, in order to absorb the energy of incoming granules and prevent excessive bouncing, but visually uniform to simplify the image analysis tasks. A prototype calibration mat was created using green artificial turf (carpet), with 7 square elements of 0.5 × 0.5 m each. A numerical label with 2 digits was placed over each grid element. Fig. 1 shows the prototype calibration mat.

2.1. Processing overview

The purpose of the ACFert system is for regular users acquiring images from a stand up position (without the use of an elevated platform) with a standard camera (on a mobile device). Considering the camera field of view and that nearly vertical observations are required to avoid excessive image deformation, the coverage of the calibration mat is limited to only a few grid elements per image. It is therefore considered that for the prototype calibration mat, each image covers between 1 and 3 grid elements, including the corresponding labels. A number of images is thus required to cover the whole calibration mat, preferably with multiple observations for each grid element.

Each image is processed independently, providing as output two numerical values for each grid element present in the image – the number of fertilizers/seeds counted, and its numerical label. A schematic overview of the image processing strategy is presented in Fig. 2, which includes the following tasks: image segmentation; grid detection; object identification and counting; labelling and aggregation of results. Each component is described in detail in the following sections, illustrated with an example – a test case image with 2 elements (quadrilaterals, corresponding to 0.5 × 0.5 m squares). A final processing stage involves the aggregation of the results produced for individual images.

2.2. Image segmentation

The goal of the image processing stage is to extract 2 binary images – one associated with the yellow component ($\mathbf{IB_y}$) of the image (grid lines and labels) and another one associated with the white/light brown component ($\mathbf{IB_w}$) of the image (objects of interest and often also some background noise).

The original RGB image is initially converted to the HSV model (Gonzalez et al., 2009), as the colour information is associated with only two components (H-Hue and S-Saturation, in the [0,1] range), and detached from the intensity component (V-Value). An iterative process is applied to obtain an initial version of $\mathbf{IB_y}$ ($\mathbf{IB_y^0}$). The binarization is performed using equation (1) and the initial values $t_{Min} = 0$ and $t_{Max} = 0.25$.

$$\mathbf{IB_y^0} = (H > t_{Min}) \text{ AND } (H < t_{Max}) \text{ AND } (S > 0.2) \quad (1)$$

The percentage of pixels ON after this initial binarization is computed, and while it is below 3%, the parameter t_{Max} is incremented by 0.005 ($t_{Max} = t_{Max} + 0.005$), and the process repeated.

The binary image with the white (or light brown) component ($\mathbf{IB_w}$) is obtained from the original RGB image (R-Red, G-Green, B-Blue) in 8bits (intensity levels in [0,255]), using Eq. (2).

$$\mathbf{IB_w} = (2 * G - R - B < 1) \text{ AND } (R > 200) \text{ AND } (B > 200) \quad (2)$$

Fig. 3 shows an example of the image segmentation process – the original image (a), binary images with yellow component ($\mathbf{IB_y}$) (b) and binary images with white/light brown component ($\mathbf{IB_W}$) (c).

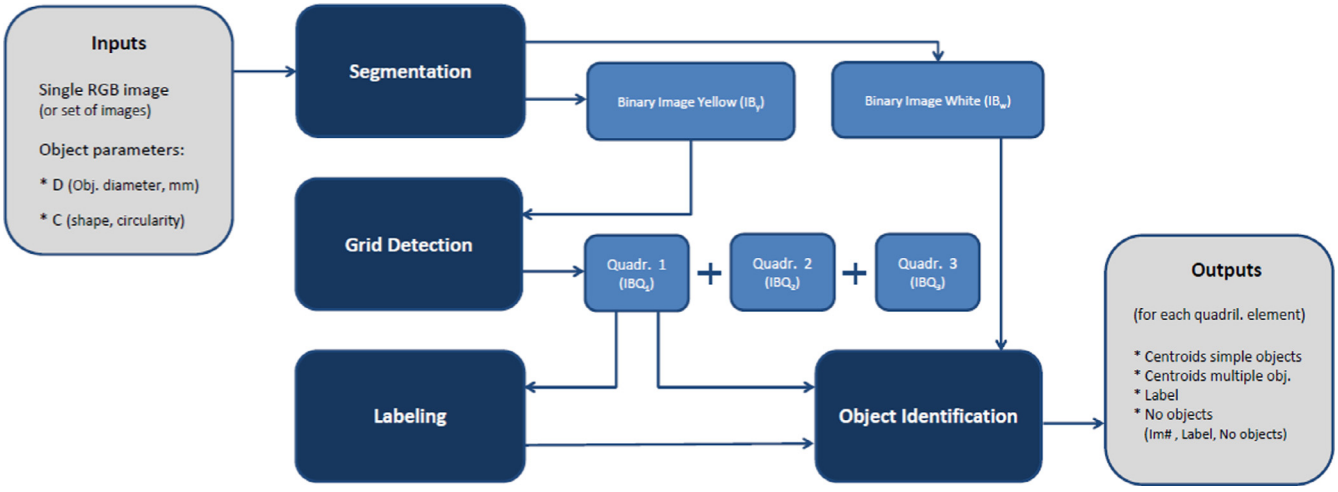

Fig. 2. Schematic overview of the processing tasks.

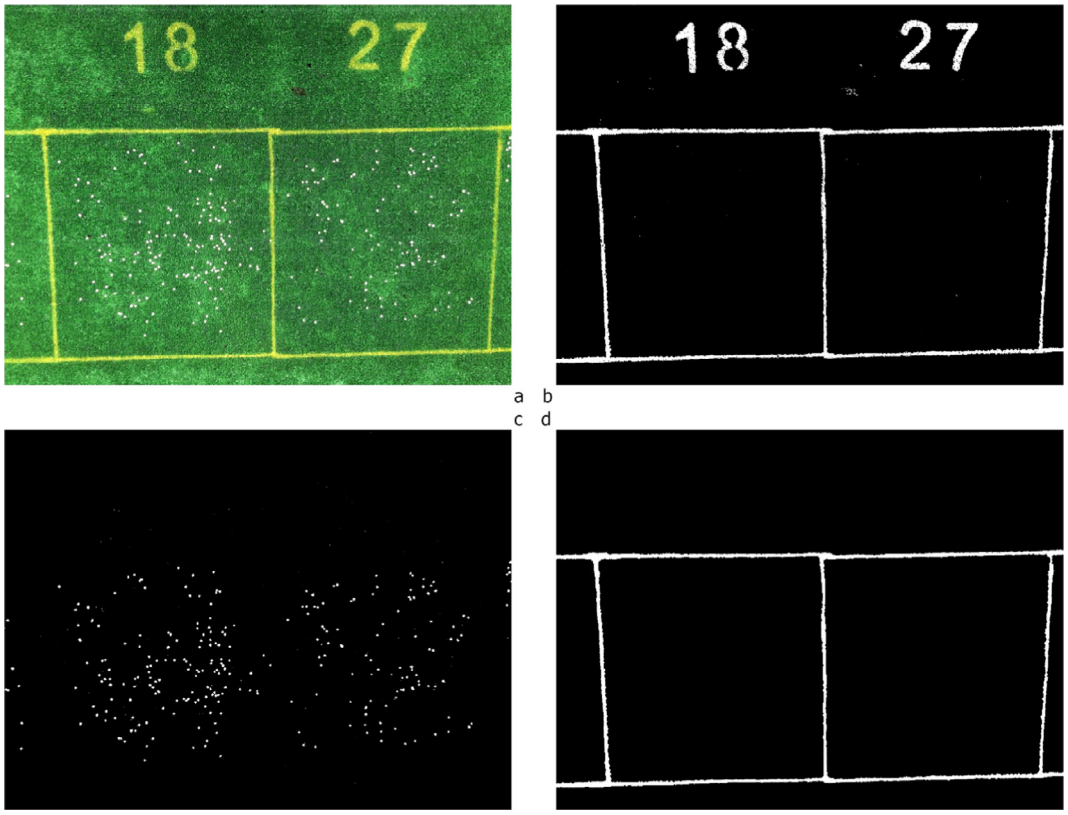

Fig. 3. Example of the image segmentation process: original image (a), binary images with yellow (b) and white/light brown (c) components, image with largest object in $\mathbf{IB_y}$ (d). (For interpretation of the references to colour in this figure legend, the reader is referred to the web version of this article.)

2.3. Grid detection

The detection of the grid in the image is based exclusively on the binary image $\mathbf{IB_y}$. The first step is to obtain a binary image with a single object ($\mathbf{IB_{y1}}$) – the grid, such as that presented in Fig. 3d). The following mathematical morphology operations (Gonzalez et al., 2009) are applied to $\mathbf{IB_y}$ in succession, using the MATLAB implementations (Mathworks, 2017):

- Closing using a 3-pixel radius disk as structuring element;
- Closing using a cross (3-pixel thickness, 15-pixel length) as structuring element;
- Extraction of the single largest object (considering a 8-neighborhood);
- Closing using a 5-pixel radius disk as structuring element;
- Extraction of the single largest object (considering a 8-neighborhood);

The resulting image ($\mathbf{IB_{y1}}$) is then subjected to a thinning process (Lam et al., 1992), using the MATLAB implementation (Mathworks, 2017). The result is a binary image with 1-pixel thick lines, which generally follow the grid. However, due to image noise and irregularities in the grid itself, these lines are not straight and require further processing. The image $\mathbf{IB_{y1}}$ for the test case is presented in Fig. 4(a).

The Hough Transform (Duda and Hart, 1972) is computed for image $\mathbf{IB_{y1}}$, using the MATLAB implementations (Mathworks, 2017). The most relevant line segments present in the image are extracted using an iterative process, by decreasing a tolerance factor in regards to the maximum value of the Hough Transform, assuring that at least 20 line segments are extracted. Each line segment is evaluated considering its angle (θ), with the image vertical axis used as reference, and labelled as nearly vertical for $|\theta| < 15^{\circ}$, nearly horizontal for $|\theta| > 85^{\circ}$, or rejected for other values of θ. The tolerance for vertical lines is higher due to the panoramic distortion that is often present in the images. The result for the test case is presented in Fig. 4(b), with the 6 longest line segments in thick yellow and the remaining line segments in thin green. The 2 most relevant horizontal line segments are extracted – 1 from the bottom and 1 from the top of the image region covered by the grid. A validation process is carried out for nearly vertical line segments (for example removing very close nearly parallel line segments). The result at this stage for the test case is presented in Fig. 4(c), where the 2 near-horizontal line segments are presented in yellow and the valid near-vertical line segments in cyan. The final stage is to define lines that contain these segments and to compute the intersections of these lines, thus defining the grid. The result for the test case illustrating the method is presented in Fig. 4(d).

The grid detection process described defines between 1 and 3 quadrilateral regions. A binary image is created for each quadrilateral region detected ($\mathbf{IBQ_1}$, $\mathbf{IBQ_2}$ and $\mathbf{IBQ_3}$), with $\mathbf{IBQ_2}$ and $\mathbf{IBQ_3}$ set to void if appropriate.

2.4. Object identification and counting

For the object identification process a size and a shape parameter are required. The size parameter is the average or expected diameter D (in mm) of the objects of interest. The shape parameter (C) is related to the circularity of the objects, defined as the ratio between long and short axis of an elliptical object (C = 1 for circular objects). For the test case illustrating the method the values used were D = 4.5 and C = 1 (nitro).

Each quadrilateral region identified ($\mathbf{IBQ_i}$, with i = 1, 2, 3) is processed separately. A binary image $\mathbf{IB_{wi}}$ is obtained as the product of images $\mathbf{IB_w}$ and $\mathbf{IBQ_i}$. An average scale (S) is computed (in pixels/mm), using $\mathbf{IBQ_i}$ and the reference grid element size (0.5 × 0.5 m for the calibration mat used). The average object diameter and minimum accepted distance between centroids are computed in pixels, and used to

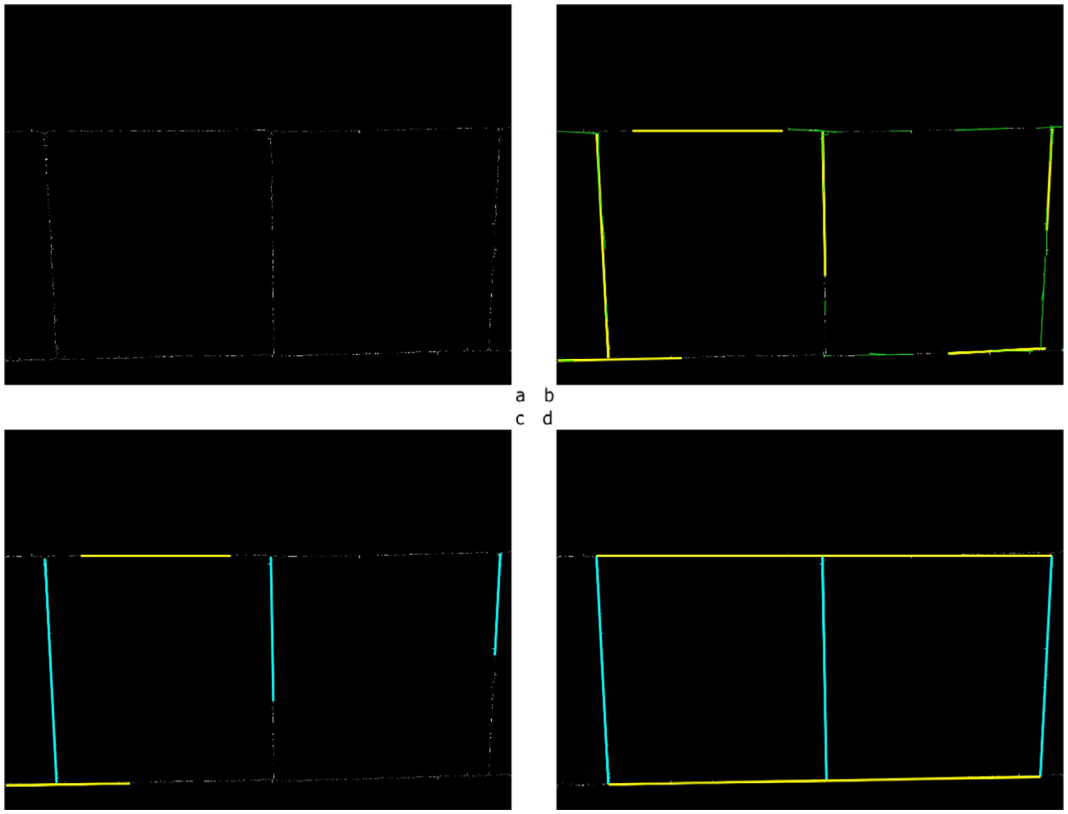

Fig. 4. Example of the grid detection process: binary image with the thinned grid (a), overlaid with line segments extracted with the Hough Transform (b-c, see text for details) and final grid (d).

define the size of a disk structuring element (SE). An erosion operation is applied to $\mathbf{IB_{wi}}$ using SE, and the centroids of all separate objects in the resulting image are computed (considering a 8-neighborhood). Centroids that are too close together (below the minimum accepted distance) are removed. Objects that have a major axis above a threshold value (computed from C, D, and S) are considered as multiple objects (2 + objects grouped together).

Two sets of centroid coordinates are provided – one for simple objects and another for multiple objects. It is possible that multiple objects refer to 3 or more individual objects, but they are nevertheless considered to refer to 2. The total number of objects is thus computed as the number of simple objects plus 2 times the number of multiple objects. The results for the test case are presented in Fig. 5. The centroids are marked in red for grid cell # 18 and in blue for grid cell # 27, with crosses for single objects and circles over crosses for multiple objects. There are 2 multiple objects near the centre of the grid cell # 27. The total number of objects identified were 150 (#18) and 99 (#27), which is very close to the reference values expected (150 and 100).

2.5. Labelling and aggregation of results

A sub-image above each quadrilateral region is extracted to identify and recognise the 2 digits that form its label. A function was developed for this purpose, using a small number of training images and 7 variables. The labels recognised for the test case are presented in Fig. 5, in white over a brown background, just above the grid cell. The total number of objects is presented alongside, in black over a green background.

The output for an image can include the location of the centroids for simple or multiple objects, but in its simplest form is just a pair of numerical values for each grid cell available – the label and number of objects.

As the purpose of the ACFert system is to process a group of images automatically, an aggregation of results procedure was developed. A set of images is initially selected. A three columns matrix is produced with (1) the 2 final digits of the image file name, (2) the grid label – 2 digits, (3) the number of objects counted. Each image contributes with up to 3 lines for the output matrix (1 for each grid cell processed). The user can inspect the data and correct for possible errors (for example in the label identification stage). Once it is validated, an aggregated matrix is created with the values combined for each grid cell, including the number of observations, mean and median values, etc.

2.6. ACFert evaluation: Experimental design

The ACFert'performance for automatic granules detection were evaluated using a set of manual counting measurements. The ACFert was tested with two common agricultural dry granules used worldwide with the broadcaster spreaders: the nitrate fertilizer "Nitrolusal" with a nitrogen rate of 27% (Nitro) and seeds of wheat (Wheat). The fertilizer is white-coloured and rounded shape (shape parameter C = 1), with an average diameter of 4.5 mm, while the wheat granules are brownish and much more angular shaped (shape parameter C = 1.2) with an average diameter of 3.5 mm (Table 1).

The granules used in the experiment have a reasonably high heterogeneity in size and shape. For Nitro, the average volume was 18.0 mm^3, with a coefficient of variation of 49.7%, and the average eccentricity of the observed 2D ellipses was 0.54 (values estimated from a sample of 1265 granules). For wheat, the average volume was 11.8 mm^3, with a coefficient of variation of 64.5%, and the average eccentricity of the observed 2D ellipses was 0.89 (values estimated from a sample of 1442 granules).

The ACFert was tested with a pre-defined number of fertilizers/seeds placed over each quadrilateral element of the grid (Fig. 1) before image acquisition (Table 1). The number of fertilizer/seed granules in each square used to test the ACFert, represents the range of plausible

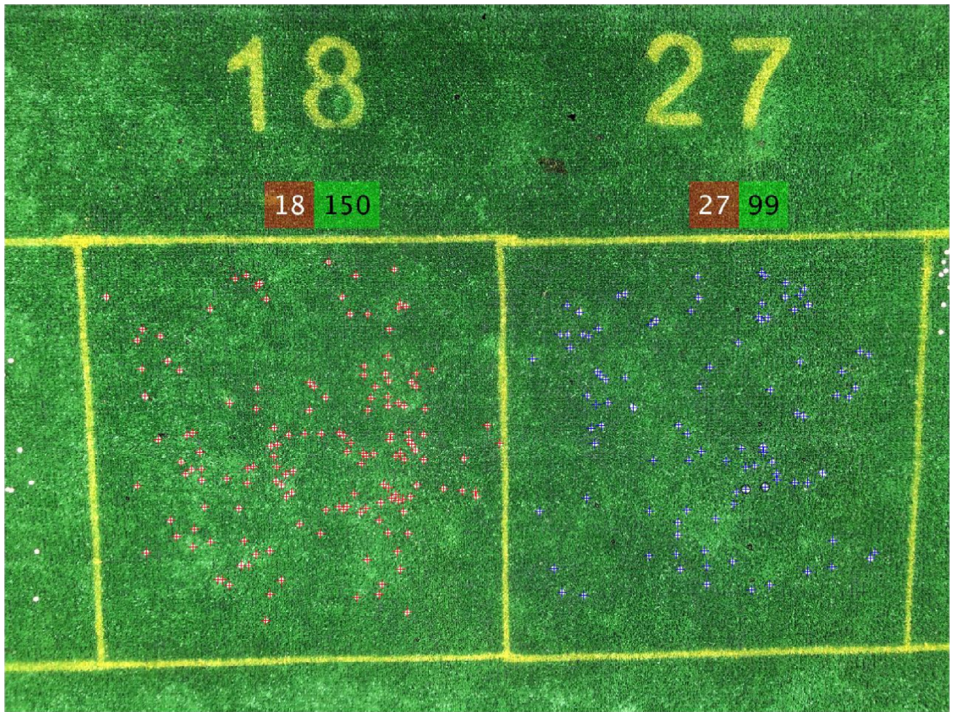

Fig. 5. Identification and counting of the objects on grid cells # 18 and #27.

Table 1
Fixed granules rate tests allocated to each grid and the equivalent agronomic application of nitrogen and wheat seeds.

	Mat element number						
Variables	**9**	**18**	**27**	**36**	**45**	**71**	**41**
Manual countings							
N° granules	200	150	100	350	50	300	250
Rate (grains/m^2)	800	600	400	1400	200	1200	1000
Fertilizer							
Mass of Fertilizer (kg/ha)	800	600	400	1400	200	1200	1000
Nitrogen rate (kg/ha)	216	162	108	378	54	324	270
Wheat Seeds							
Application rate (kg/ha)	240	180	120	420	60	360	300

values for agronomic application of both products. Therefore, a fixed application rate tests were conducted in the range between 54 and 378 kg/ha of nitrogen and between 60 and 420 kg/ha of seeds rate for wheat.

Two mobile devices were used for the image acquisition: a Samsung Galaxy (Sam) with a camera resolution of 12 MB (4128 × 3096 pixels), an Apple iPhone 5S (iPho) with a camera resolution of 8 MB (3264 × 2448 pixels).

A total of 14 experiments (takes) were carried out in 3 different days using the calibration mat (Fig. 1). The pre-defined number of fertilizers/seeds is placed over each quadrilateral element of the grid and a sequence of images is acquired with a device (forming a take). The acquisition of a set of images with the same configuration but a different device results in a new take. The position of the fertilizers/seeds in the mat is then shuffled, without changing the reference values, and a new set of images is acquired for a new take.

The differences between the manual counting and ACFert measurements were presented for each quadrilateral in terms of absolute relative error (RE) ± the standard deviation (SD) expressed in percentage.

To check possible differences among experimental image acquisition conditions (takes, devices, images covering two or three quadrilaterals, illumination, etc.), on the mean RE between manual counting and ACFert measures, we performed an one-way analysis of variance (ANOVA). Everywhere in the text the difference between two subsets of data is considered statistically significant if the F-test from ANOVA gives a significance level P (P value) below 0.05.

3. Results

3.1. Results of different experiments

The statistical results for the experiments and devices used in each experiment, as well as the number of images acquired covering 2 and 3 quadrilateral elements, are presented in Table 2 for fertilizer (Nitro) and Table 3 for seeds (Wheat). The total number of quadrilateral elements observed in each take is also presented in Tables 2 and 3.

A total of 185 images (125 Nitro and 60 for wheat) were used with a total of 498 (Nitro 279 Nitro, Wheat 119) quadrilateral elements observed and analysed. Most of these images have 2 quadrilateral grid elements, but some of the Nitro images (29) have 3 grid elements.

The overall mean differences between counting and derived from ACFert (RE), were 0.75 ± 0.75% for Nitro and 2.12 ± 1.68% for wheat and this difference is statistically significant ($p < 0.000$). The maximum RE were 2.67% for Nitro and 7.84% for Wheat both images acquired with the Samsung device (Tables 2 and 3).

In the ACFert tests with Nitro, the conditions of the image acquisition (experiments, number of quadrilateral and device), did not have significant impact on the mean RE (Table 2). Despite the mean RE significant differences presented for the image conditions among the quadrilateral tested, it is possible to infer that the ACFert produces always very low means RE, associated to a low SD. The mean RE for the images cover 2 quadrilaterals (0.69 ± 0.76%) were lower than the one for the 3 quadrilateral images (0.88 ± 0.7%), but this difference is not statistically significant. The images acquired with both devices (iPhone and Samsung) had a mean RE close to 0.75 ± 0.75%, and a maximum RE value of 2.67% recorded with the Samsung. The consistency and robustness of the results suggest that ACFert can produce accurate results in different image acquisition conditions.

Table 2
Statistical results for the different conditions used in the image acquisition of fertilizer (Nitro) on the relative error between manual counting and ACFert measures in each quadrilateral.

Variable	Statistics		Mat element number						
		Overall	**9**	**18**	**27**	**36**	**41**	**45**	**71**
Manual counting		–	200	150	100	350	250	50	300
Takes (experiments) carried out									
Takes	Nobs	8	8	8	8	8	8	8	8
Takes (1)	Mean RE	0.75 ^{ns}	1.80 ^{ns}	0.57 ^{ns}	0.78 ^{ns}	0.63 *	0.60 ^{ns}	0.80 *	0.52 ^{ns}
	(SD)	(0.75)	(0.57)	(0.65)	(0.74)	(0.52)	(0.57)	(1.00)	(0.39)
Quadrilateral (Q) in the image									
2Q	Nobs	192	16	32	32	32	16	32	32
3Q	Nobs	87	6	10	17	15	8	19	12
2Q	Mean RE	0.69	2.00	0.542	0.78	0.42	0.43	0.64	0.54
	(SD)	(0.76)	(0.45)	(0.62)	(0.79)	(0.40)	(0.56)	(0.96)	(0.38)
3Q	Mean	0.88	1.25	0.67 ^{ns}	0.76 ^{ns}	1.07 ^{ns}	0.95	1.01	0.44
	(SD)	(0.73)	(0.52)	(0.77)	(0.66)	(0.50)	(0.42)	(1.05)	(0.43)
ANOVA F test P level		ns	*	ns	ns	**	*	*	ns
Device for image acquisition									
iPhone	Nobs	138	11	21	24	23	12	25	22
Sam	Nobs	141	11	21	25	24	12	26	22
iPhone	Mean RE	0.76 (0.75)	1.59	0.50	0.83	0.71	0.57	0.90	0.42
	(SD)		(0.63)	(0.51)	(0.76)	(0.57)	(0.60)	(1.04)	(0.39)
Sam	Mean RE	0.74	2.00	0.63	0.72 (0.74)	0.55 (0.48)	0.63 (0.55	0.63 (0.96)	0.61 (0.38)
	(SD)	(0.76)	(0.44)	(0.77)					
ANOVA F test, P level		ns	ns	ns	ns	ns	ns	ns	ns
iPhone	Maximum RE	2.50	2.50	1.33	2.00	1.71	1.60	2.04	1.33
Sam	Maximum RE	2.67	2.50	2.67	2.00	1.43	1.60	1.33	1.33

ANOVA F test is the statistical significance level of mean differences: no significant (ns), significant at 5% (*), 1% (**) and0.1% (***). (1) the label after the mean indicates the significant level of the mean comparison among the experiments.
RE: Relative error between manual countings and ACFert measurements.

In the tests with Wheat, both the experiments and the device used for image acquisition had a significant impact on the mean RE. The standard error among the experiments and devices, for each quadrilateral element, were much higher than the ones obtained in the experiments with Nitro. The images for wheat acquired with Samsung device had a mean RE of 2.88 ± 1.81%, which were significantly higher than the mean RE for the images acquired with the iPhone (1.29 ± 1.03%).

Despite the statistical significant impact of the conditions of the image acquisition on the mean RE, suggesting low robustness and consistency of the ACFert for wheat, these results should be relativized considering the very low values of mean RE ($\leq$2.88 ± 1.81%), which represents only a very small difference in the number of granules. The higher differences difference for Wheat, compared with Nitro, could be explained by its non-cylindrical shape, lower contrast between the seeds and the mat, and higher particle overlap that could not be well separated. Also, the variability of the landing position (verticality) of the wheat granules in the top of the mat could disrupt the identification.

Table 3
Statistical results for the different conditions used in the image acquisition of seeds (Wheat) on the relative error between manual countings and ACFert measures in each quadrilateral.

Variable	Statistics		Mat element number						
		Overall	**9**	**18**	**27**	**36**	**41**	**45**	**71**
Manual counting		–	200	150	100	350	250	50	300
Takes (experiments) carried out									
Takes	Nobs	6	6	6	6	6	6	6	6
2Q	Nobs	119	10	20	20	20	9	20	20
Stat (1)	Mean RE	2.12 *	2.00 ^{ns}	2.03 ^{ns}	1.36 ^{ns}	1.76 *	2.56 ^{ns}	3.14 *	2.17 *
	(SD)	(1.68)	(1.15)	(1.13)	(1.40)	(1.27)	(1.43)	(2.50)	(1.73)
Device for image acquisition									
iPhone	Nobs	57	5	10	10	10	3	10	9
Sam	Nobs	62	5	10	10	10	6	10	11
iPhone	Mean RE	1.29	2.00	1.67	0.98	0.97	2.53	1.57	0.49
	(SD)	(1.03)	(1.41)	(0.2.4)	(1.08)	(0.63)	(0.23)	(1.24)	(0.41)
Sam	Mean RE	2.88	2.00 ^{ns}	2.40 ^{ns}	1.74 ^{ns} (1.64)	2.55 * (1.28)	2.60 ^{ns} (1.80)	4.71 (2.50	3.54 (0.96)
	(SD)	(1.81)	(1.00)	(1.38)					
ANOVA F test P level		**	ns	ns	ns	*	ns	**	***
iPhone	Maximum RE	3.92	3.00	2.67	3.26	2.00	2.80	3.92	1.17
Sam	Maximum RE	7.84	3.50	4.00	4.35	4.86	6.00	7.84	5.28

ANOVA F test is the statistical significance level of mean differences: no significant (ns), significant at 5% (*), 1% (**) and0.1% (***). (1) the label after the mean RE indicates the significant level of the mean comparison among the experiments.
RE: Relative error between manual counting and ACFert measurements.

Table 4
Unaggregated output results for an experiment with nitro – take #3.

ImNo	Quad	Count	ImNo	Quad	Count	ImNo	Quad	Count	ImNo	Quad	Count
61	9	204	65	71	301	70	27	99	76	45	49
61	18	149	66	71	299	70	36	349	76	71	300
62	18	150	66	41	250	71	18	150	76	41	246
62	27	99	67	71	300	71	27	99	77	27	98
63	27	99	67	41	250	72	9	205	77	36	349
63	36	349	68	45	49	72	18	149	77	45	48
64	36	351	68	71	299	75	45	49	78	9	203
64	45	49	69	36	349	75	71	298	78	18	149
65	45	49	69	45	49	75	41	248	78	27	99

Table 5
Aggregated results for an experiment with nitro – take #3.

	Mat element number						
Statistics	9	18	27	36	41	45	71
Manual counting	200	150	100	350	250	49	300
No Images	3	5	6	5	4	7	6
Mean counting	204.0	149.4	98.8	349.4	248.5	48.9	299.5
St.Dev.	1.00	0.55	0.41	0.89	1.92	0.38	1.05
Minimum	203	149	98	349	246	48	298
Median counting	204	149	99	349	249	49	299.5
Maximum	205	150	99	351	250	49	301
Relative error (RE) (%)	1.30	0.30	0.00	1.10	0.40	0.00	0.20

The relative error (RE), was computed as |Median - Ref.V.|/Ref.V (%).

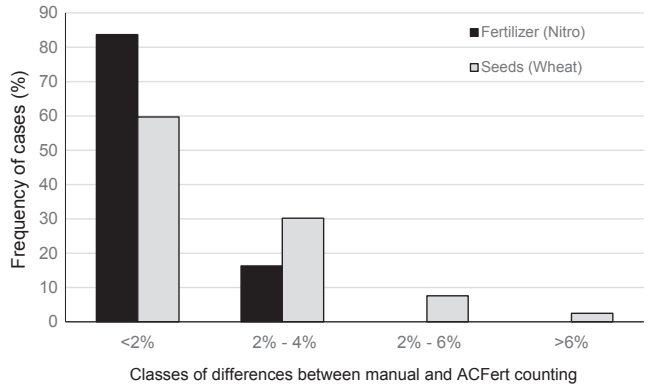

Fig. 6. Overall relative error between manual and ACFert countings for Fertilizer (Nitro, 279 observations) and seeds (Wheat, 119 observations).

3.2. Detailed results for one take

A take (#3) with 16 images for nitro acquired with the iPhone device, was selected for a more detailed presentation of results provide by the ACFert. Take #3 includes the test case image presented in Figs. 3–5. Table 4 presents the initial output provided by the ACFert system after processing all 16 images. Some of these images have 2 quadrilateral grid elements (12) and some (4) have 3 grid elements, thus resulting in a total of 36 grid elements observed. The output is a 36 × 3 matrix, which for compactness is presented here re-structured in 9 × 12 format.

The aggregated results produced for take #3 are presented in Table 5. As it happens, the output provided by the system corresponds to only the first 7 lines in Table 5 – the quadrilateral grid element number (Quad.), number of observations (No.Obs), mean value, standard deviation (St.Dev.); minimum, median and maximum values. These values are presented in Table 5 in raw, with variable significant figures, depending on the number of observations available. As this is an experimental evaluation with reference values available (Ref.V.), the relative errors were also included in Table 5 (last row).

3.3. Overall accuracy

Fig. 6 presents the overall accuracy based on the RE of the ACFert for the fertilizer and seeds. For the fertilizer Nitro, which have 279 observations (quadrilateral elements), the descriptive statistics show that 100% of cases had RE below 4%. The tests performed for Wheat with 119 observations (quadrilateral elements), recorded 10% of the cases with RE higher than 4%, with only 1 case of a difference higher than 6% (Fig. 6).

The results suggest that the ACFert is a robust portable system to provide consistent and accurate information for spreader pattern calibration.

4. Conclusions

An automatic calibration system (ACFert) based on image processing techniques was presented for the assessment of the lateral pattern of distribution of agricultural spreaders. The system was tested with a total of 185 images, with 398 quadrilateral elements, that cover two different agricultural particles in different applications rates, as well as several conditions of image acquisition. The overall mean differences between manual counting and derived from ACFert, were 0.75 ± 0.75% for nitrogen fertilizers with rounded shaped granules, and 2.12 ± 1.68% with elliptical shaped seeds of wheat.

The ACFert tests performed for algorithm development and accuracy assessment, were based on a test calibration mat that follow the ISO international standard calibration norms (0.5 m × 0.5 m). A more complete mat would have a larger number of elements, numbered sequentially. Furthermore, the ACFert'algorithms system can be adapted to accommodate the main rules of other referred international standard for spreader calibration, such as the size of the quadrilateral elements and their transverse row spacing. However, further testing is required, with a larger number of agricultural granules and other camera devices. For fertilizers or seeds with smaller particle size, a calibration mat with thinner fibbers should be used. Also, the color of the mat tested (green) could be unsuitable for some fertilizers.

The accuracy and robustness of the results of the ACFert justify their use for providing enhanced support to spreader calibration with agronomic, economic and environmental benefits for a range of potential users. For farmers, the ACFert can be used as a routine operation to control the uniformity of fertilizer and seeds according to machine spreaders, properties of agricultural granules and climate conditions during the application. For machine developers, ACFert can be used to support innovative processes in machine design and for spreaders manufactures, in order to produce spreading tables which link fertilizer properties to the machine settings and for machine design. Future applications of the ACFert implemented on a smartphone can be particularly interesting to provide full calibration of spreaders.

References

Abbou-ou-cherif, E.M., Piron, E., Chateauneuf, A., Miclet, D., Lenain, R., Koko, J., 2017. On-the-field simulation of fertilizer spreading: Part 1-Modeling. Comput. Electron.

Agric. 142, 235–247.
Aphale, A., Bolander, N., Park, J., Shaw, L., Svec, J., Wassgren, C., 2003. Granular fertiliser particle dynamics on and off a spinner spreader. Biosyst. Eng. 85, 319–329.
ASABE, 2004. Procedure for measuring distribution uniformity and calibrating granular broadcast spreaders.
Back, S.W., Yu, S.H., Kim, Y.J., Chung, S.O., Lee, K.H., 2014. An image-based application rate measurement system for a granular fertilizer applicator. Trans. ASABE 57, 679–687.
Cool, S., Pieters, J., Mertens, K.C., Hijazi, B., Vangeyte, J., 2014. A simulation of the influence of spinning on the ballistic flight of spherical fertiliser grains. Comput. Electron. Agric. 105, 121–131.
Cool, S.R., Pieters, J.G., Seatovic, D., Mertens, K.C., Nuyttens, D., Van De Gucht, T.C., Vangeyte, J., 2017. Development of a stereovision-based technique to measure the spread patterns of granular fertilizer spreaders. Sensors (Basel) 17.
Cool, S.R., Pieters, J.G., Van Acker, J., Van Den Bulcke, J., Mertens, K.C., Nuyttens, D.R.E., Van De Gucht, T.C., Vangeyte, J., 2016a. Determining the effect of wind on the ballistic flight of fertiliser particles. Biosyst. Eng. 151, 425–434.
Cool, S.R., Vangeyte, J., Mertens, K.C., Nuyttens, D.R.E., Sonck, B.R., Van de Gucht, T.C., Pieters, J.G., 2016b. Comparing different methods of using collecting trays to determine the spatial distribution of fertiliser particles. Biosyst. Eng. 150, 142–150.
Duda, O.R., Hart, P., 1972. Use of the Hough transformation to detect lines and curves in pictures. Commun. ACM 15, 11–15.
Gonzalez, R.C., Woods, R.E., Eddins, S.L., 2009. Digital Image Processing Using MATLAB, second ed. Gatesmark Publishing.
Griffis, C.L., Ritter, D.W., Matthews, E.J., 1983. Simulation of rotary spreader distribution patterns. Trans. Asae 26, 33–37.
Grift, T., 2000. Spread Pattern Analysis Tool (SPAT): I. Development and theoretical examples.
Grift, T.E., Hofstee, J.W., 1997. Measurement of velocity and diameter of individual fertilizer particles by an optical method. J. Agric. Eng. Res. 66, 235–238.
Hensel, O., 2003. A New Methodology for Mapping Fertilizer Distribution. ASAE, St. Joseph, MI.
Hijazi, B., Cool, S., Vangeyte, J., Mertens, K.C., Cointault, F., Paindavoine, M., Pieters, J.G., 2014. High speed stereovision setup for position and motion estimation of fertilizer particles leaving a centrifugal spreader. Sensors 14, 21466–21482.
Hijazi, B., Vangeyte, J., Cointault, F., Dubois, J., Coudert, S., Paindavoine, M., Pieters, J., 2011. Two-step cross correlation-based algorithm for motion estimation applied to fertilizer granules' motion during centrifugal spreading. Opt. Eng. 50, 067002.
Hofstee, J.W., Huisman, W., 1990. Handling and spreading of fertilizers Part 1: Physical properties of fertilizer in relation to particle motion. J. Agric. Eng. Res. 47, 213–234.
Inns, F.M., Reece, A.R., 1962. The theory of the centrifugal distributor II: Motion on the disc, off-centre feed. J. Agric. Eng. Res. 57, 3621–3638.
Jones, J.R., Lawrence, H.G., Yule, I.J., 2008. A statistical comparison of international fertiliser spreader test methods — Confidence in bout width calculations. Powder Technol. 184, 337–351.
Lam, L., Lee, S.W., Suen, C.Y., 1992. Thinning methodologies-a comprehensive survey. IEEE Trans. Pattern Anal. Mach. Intell. 14, 869–885.
Lawrence, H.G., Yule, I.J., Coetzee, M.G., 2007. Development of an image-processing method to assess spreader performance. Trans. ASABE 50, 397–407.
Mathworks, 2017. . MATLAB and Image Processing Toolbox Release 2017a, second ed. The MathWorks, Natick, Massachusetts, United States.
Mennel, R.M., Reece, A.R., 1963. The theory of the centrifugal distributor III: Particles trajectories. J. Agric. Eng. Res. 8, 78–84.
Olieslagers, R., Ramon, H., DeBaerdemaeker, J., 1996. Calculation of fertilizer distribution patterns from a spinning disc spreader by means of a simulation model. J. Agric. Eng. Res. 63, 137–152.
Parish, R.L., 2003. Effect of impeller angle on pattern uniformity. Appl. Eng. Agric. 19, 531–533.
Parish, R.L., 2006. Review of granular applicators for turfgrass. HortTechnology 16, 533–538.
Patterson, D.E., Reece, A.R., 1962. The theory of the centrifugal distributor I: Motion on the disc, near-centre feed. J. Agric. Eng. Res. 7, 232–240.
Reumers, J., Tijskens, E., Ramon, H., 2003. Experimental characterisation of the cylindrical distribution pattern of centrifugal fertiliser spreaders: towards an alternative for spreading hall measurements. Biosyst. Eng. 86, 431–439.
Shi, Y.Y., Chen, M., Wang, X.C., Odhiambo, M.O., Ding, W.M., 2018. Numerical simulation of spreading performance and distribution pattern of centrifugal variable-rate fertilizer applicator based on DEM software. Comput. Electron. Agric. 144, 249–259.
Van Liedekerke, P., 2007. Study of the granular fertilizers and the centrifugal spreader using Discrete Element Method (DEM) simulations, Bio-ingenieurswetenschappen. Catholic University of Leuven,, Belgium.
Van Liedekerke, P., Tijskens, E., Dintwa, E., Anthonis, J., Ramon, H., 2006. A discrete element model for simulation of a spinning disc fertilizer spreader I. Single particle simulations. Powder Technol. 170, 71–85.
Van Liedekerke, P., Tijskens, E., Dintwa, E., Rioual, F., Vangeyte, J., Ramon, H., 2009. DEM simulations of the particle flow on a centrifugal fertilizer spreader. Powder Technol. 190, 348–360.
Zhou, L., Ma, M., Yuan, Y., Zhang, J., Dong, X., Wei, C., 2017. Design and test of fertilizer mass monitoring system based on capacitance method. Trans. Chinese Soc. Agric. Eng. 33, 44–51.